Supplementary Information (SI) for Inorganic Chemistry Frontiers.

## Supporting Information

# Tuning photochromism and photomagnetism *via* diverse bimetallic cyanido viologen hybrid materials

Xin-Xin Jin,[a] Zhen Shao,[e] Peng-Xiang Fu,[a] Yi-Fan Deng,[a] Qi Sui,[f] Yi-Han Wang,[a] Jin Xiong,*[b] Bing-Wu Wang,*[a, c] Zhe-Ming Wang[a] and Song Gao*[a, d]

[a] *Beijing National Laboratory for Molecular Science, Beijing Key Laboratory for Magnetoelectric Materials and Devices, College of Chemistry and Molecular Engineering, Peking University, Beijing 100871, P. R. China. Email: wangbw@pku. edu.cn; gaosong@pku.edu.cn*

[b] *Department of Chemistry, Carnegie Mellon University, Pittsburgh, PA 15213, United States. Email:* jinxiong@andrew.cmu.edu

[c] *School of Chemical Engineering, Guizhou Minzu University, Guiyang 550025, P. R. China.*

[d] *Key Laboratory of Bioinorganic and Synthetic Chemistry of Ministry of Education, LIFM, School of Chemistry, IGCME, Sun Yat-sen University, Guangzhou 510275, P. R. China.*

[e] *State Key Laboratory of Fine Chemicals, Dalian University of Technology, Dalian 116024, P. R. China.*

[f] *Key Laboratory of Surface & Interface Science of Polymer Materials of Zhejiang Province, School of Chemistry and Chemical Engineering, Zhejiang Sci-Tech University, Hangzhou 310018, P. R. China.*

## Contents

## Experimental Section

**Materials.** All reagents and solvents were commercially available and used without further purification. Methyl viologen dichloride ($MVCl_2$) was synthesized according to literature procedures.[1]

***Caution!*** Cyanides are highly toxic and should be handled with caution.

**Synthetic Details**. Synthesis of $(MV^{II})_{0.5}[Fe^{III}Mn^{II}(CN)_6(H_2O)_2]\cdot(H_2O)_5$ (**FeMn**). An aqueous solution (5 ml) of $K_3[Fe(CN)_6]$ (66 mg, 0.2 mmol) was slowly added to an aqueous solution (5 ml) of $MnCl_2\cdot4H_2O$ (40 mg, 0.2 mmol) and $MVCl_2$ (103 mg, 0.4 mmol). The mixture was stirred for 30 min at room temperature to yield a brown suspension. After filtering off the brown precipitate, the yellow filtrate was slowly evaporated in the dark at room temperature for two weeks to yield reddish-brown block crystals. Notably, the crystals will easily weather away from the crystallization mother liquor and lose their crystalline solvents leading to structural collapse. The phase purity of the crystals was checked by PXRD. Yield: 10% based on $K_3[Fe(CN)_6]$. Elemental analysis (%) calcd for $C_{12}H_{21}N_7O_7FeMn$ ($M = 486.12$): C, 29.65; H, 4.35; N, 20.17; Fe, 11.49; Mn, 11.30. Found: C, 29.63; H, 4.10; N, 20.45; Fe, 12.10; Mn, 12.00.

Synthesis of $(MV^{II})_{0.5}[Fe^{III}Zn^{II}(CN)_6]\cdot(H_2O)_{0.5}$ (**FeZn**). An aqueous solution (2 ml) of $K_3[Fe(CN)_6]$ (66 mg, 0.2 mmol) was placed in the bottom of a glass tube, then 10 ml $H_2O$ was slowly added dropwise as a buffering solvent. Finally, an aqueous solution (2 ml) of $ZnCl_2$ (27 mg, 0.2 mmol) and $MVCl_2$ (103 mg, 0.4 mmol) was slowly added. The glass tube was sealed and put in the dark at room temperature for one week to yield dark yellow block crystals. The crystals were filtered, washed with water and ethanol, and finally dried in air. The phase purity of the crystals was checked by PXRD. Yield: 20% based on $K_3[Fe(CN)_6]$. The black sample of **FeZn-P** was obtained upon irradiation with a Xe lamp for about 1 hour at room temperature. The **FeZn-dehydrated** was obtained upon heating at 150 °C by TGA. The dark brown sample of **FeZn-UV** was obtained upon irradiation with UV light for about 1 hour at room temperature. Elemental analysis (%) calcd for $C_{12}H_8N_7O_{0.5}FeZn$ (**FeZn**, $M = 379.49$): C, 37.98; H, 2.12; N, 25.84; Fe, 14.70; Zn, 17.20. Found: C, 37.82; H, 2.01; N, 26.35; Fe, 14.40; Zn, 15.70. Elemental analysis (%) calcd for $C_{12}H_7N_7FeZn$ (**FeZn-P**, $M = 370.49$): C, 38.90;

H, 1.90; N, 26.46. Found: C, 38.57; H, 2.25; N, 25.86. Elemental analysis (%) calcd for $C_{12}H_7N_7FeZn$ (**FeZn-dehydrated**, $M = 370.49$): C, 38.90; H, 1.90; N, 26.46. Found: C, 38.63; H, 2.01; N, 26.48. IR of **FeZn** (KBr, $cm^{-1}$): 3433(br), 3126(m), 3051(m), 2925(w), 2852(w), 2376(w), 2349(w), 2297(w), 2202(m), 2165(s), 2142(s), 2119(s), 2098(s), 1722(w), 1641(s), 1564(m), 1506(m), 1448(m), 1334(m), 1267(m), 1222(w), 1184(m), 1060(w), 1039(w), 960(w), 864(w), 825(m), 802(m), 736(w), 711(w), 661(w), 597(w), 553(m), 513(m), 439(m).

Synthesis of $(MV^{II})_{0.5}[Cr^{III}Mn^{II}(CN)_6]$ (**CrMn**). The synthesis procedure was the same as **FeZn**, except that $K_3[Fe(CN)_6]$ and $ZnCl_2$ were replaced by $K_3[Cr(CN)_6]$ (65 mg, 0.2 mmol) and $MnCl_2{\cdot}4H_2O$ (40 mg, 0.2 mmol). The light-yellow needle crystals were obtained for one month in the dark at room temperature. The crystals were filtered, washed with water and ethanol, and finally dried in air. The phase purity of the crystals was checked by PXRD. Yield: 19% based on $K_3[Cr(CN)_6]$. Elemental analysis (%) calcd for $C_{12}H_7N_7CrMn$ ($M = 356.17$): C, 40.47; H, 1.98; N, 27.53; Cr, 14.60; Mn, 15.42%. Found: C, 40.13; H, 2.00; N, 27.49; Cr, 14.20; Mn, 15.50. IR of **CrMn** (KBr, $cm^{-1}$): 3138(w), 3109(w), 3088(w), 3066(w), 2160(s), 2143(s), 1932(w), 1818(w), 1784(w), 1715(w), 1649(s), 1574(m), 1516(m), 1454(m), 1332(m), 1273(m), 1230(m), 1194(m), 1061(w), 970(w), 864(w), 821(s), 804(w), 713(w), 661(w), 551(w), 523(m), 472(s).

Synthesis of $(MV^{II})_{0.5}[Cr^{III}Zn^{II}(CN)_6]$ (**CrZn**). The synthesis procedure was the same as **FeZn**, except that $K_3[Fe(CN)_6]$ was replaced with $K_3[Cr(CN)_6]$ (65 mg, 0.2 mmol). The light-yellow needle crystals were obtained for one month in the dark at room temperature. The crystals were filtered, washed with water and ethanol, and finally dried in air. The phase purity of the crystals was checked by PXRD. Yield: 24% based on $K_3[Cr(CN)_6]$. The green sample of **CrZn-P** was obtained upon irradiation with a Xe lamp for about 6 hours at room temperature. Elemental analysis (%) calcd for $C_{12}H_7N_7CrZn$ (**CrZn**, $M = 366.64$): C, 39.31; H, 1.92; N, 26.74; Cr, 14.18; Zn, 17.84. Found: C, 39.42; H, 1.99; N, 26.82; Cr, 14.10; Zn, 17.10. Elemental analysis (%) calcd for $C_{12}H_7N_7CrZn$ (**CrZn-P**, $M = 366.64$): C, 39.31; H, 1.92; N, 26.74. Found: C, 39.54; H, 1.99; N, 26.61. IR of **CrZn** (KBr, $cm^{-1}$): 3142(w), 3113(w), 3091(w), 3070(w), 2177(s), 2158(s), 1930(w), 1816(w), 1651(s), 1572(m), 1516(w), 1456(m), 1331(w), 1272(w), 1230(w), 1197(m), 972(w), 864(w), 819(s), 711(w), 659(w), 550(w), 523(m), 474(s).

**Physical Measurements.** Fourier transform infrared spectroscopy (FT-IR) was recorded in the range of 400-4000 $\mathrm{cm^{-1}}$ using KBr pellets on a Bruker Tensor 27 spectrophotometer. The CHN elemental analyses were performed on an Elementar Vario EL Cube analyzer. The elemental analyses of Fe, Mn, Zn, and Cr were measured on a Prodigy 7 ICP-OES spectrometer. Thermogravimetric analysis (TGA) was carried out on a TA SDT Q600 analyzer from 30 to 800 °C with a heating rate of 10 °C $\mathrm{min^{-1}}$ under an $N_2$ atmosphere. Power X-ray diffraction (PXRD) patterns were recorded on a PANalytical X-Pert3 Powder X-ray diffractometer using Cu K$\alpha$ radiation. Electron paramagnetic resonance (EPR) spectra were recorded on a Bruker Elexsys 580 spectrometer in the X band at room temperature. Diffuse reflectance spectra were measured at room temperature in the wavelength range of 200-2600 nm on a Shimadzu UV-3600 Plus UV-VIS-NIR spectrophotometer equipped with an integrating sphere, with $BaSO_4$ plates as references (100% reflection). X-ray photoelectron Spectrometer (XPS) studies were performed with an AXIS Supra using Al K$\alpha$ radiation ($\lambda$ = 8.357 Å). $^{57}$Fe Mössbauer spectra were recorded on a Wissel WSS-10 equipped with a temperature controller, and the isomer shift values are reported against the value of $\alpha$-Fe foil under 300 K. A CEL-HXUV300-T3 300W xenon lamp system equipped with an IR filter was used as a photoirradiation source, wherein the distance between the sample and the Xe lamp was set as 20 cm. The UV light was generated by a hand-held UV lamp (365 nm, 180 W). Quantum Design MPMSXL5 SQUID magnetometer was used to measure the dc susceptibility and magnetization of **FeZn** and **FeZn-P**, the magnetization and variant-field FC susceptibilities of **FeMn**. Other magnetic measurements were collected on the Quantum Design MPMS3 magnetometer. Diamagnetic corrections were estimated with Pascal's constants, while experimental measurements on sample holders (parafilm film, capsule and N-grease) were used for background corrections.

**X-ray Crystallography.** Single-crystal X-ray diffraction measurements were performed at 180 K and 90 K on a Rigaku Oxford diffractometer equipped with a CCD collector and graphite monochromated Mo K$\alpha$ radiation ($\lambda = 0.71073$ Å). The structures were solved by the ShelXT structure solution program using Intrinsic Phasing and refined with the ShelXL refinement package using Least Squares minimization that was implanted in Olex2. Anisotropic refinement was applied to all non-hydrogen atoms, and all hydrogen atoms were calculated geometrically. The crystal data and structure refinement data are listed in Table S1. The selected bond lengths and bond angles are listed in Table S2-S7.

**Calculations.** Periodic density functional theory (pDFT) methods were used for calculating density of states (DOS), which has been implemented in the VASP package.[2] The PBE functional for the generalized gradient approximation (GGA) was used in the description of the exchange-correlation interactions. The interactions between the valence electrons and cores were treated by the full potential projected augmented wave (PAW) pseudopotentials with an energy cutoff of 530 eV for the plane-wave expansion. The global break condition for the electronic SC-loop is 1e-6 eV.

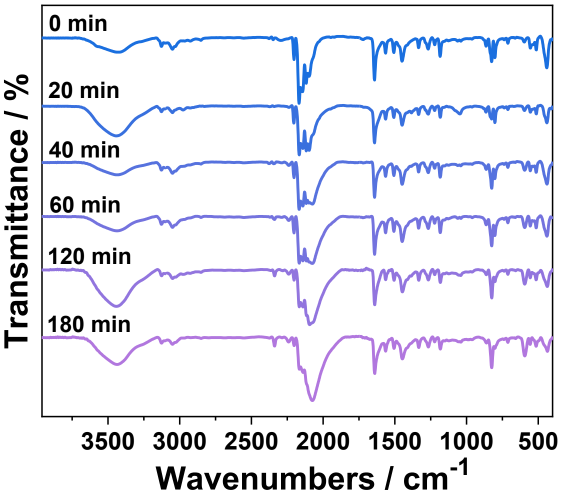

**Figure S1.** Time-dependent IR spectra of **FeZn** upon irradiation at room temperature.

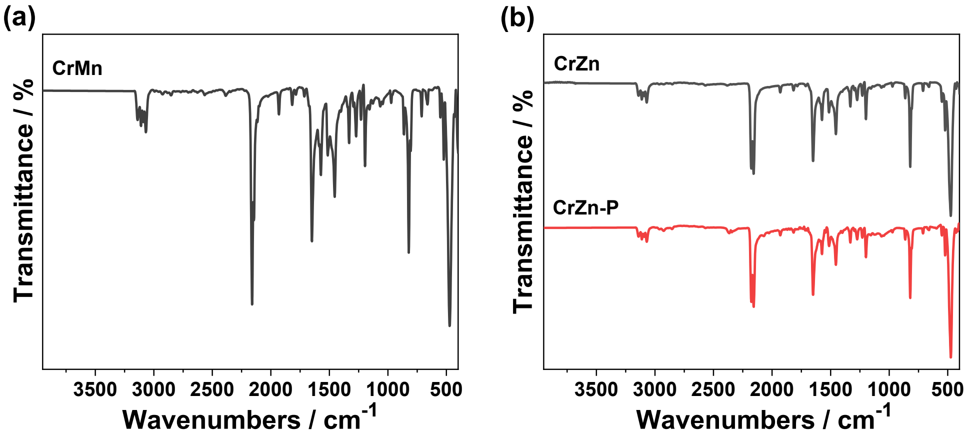

**Figure S2.** IR spectra for **CrMn** (a), **CrZn** and **CrZn-P** (b).

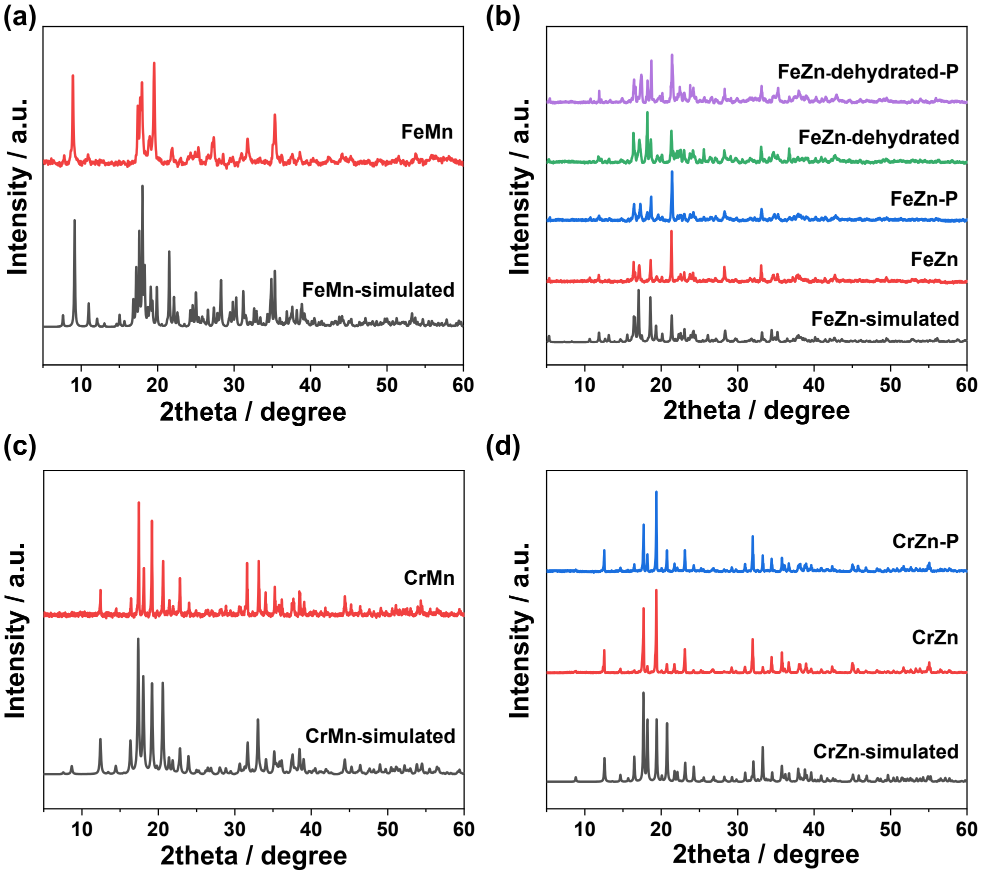

**Figure S3.** PXRD patterns for **FeMn** (a), **FeZn** (b), **CrMn** (c) and **CrZn** (d).

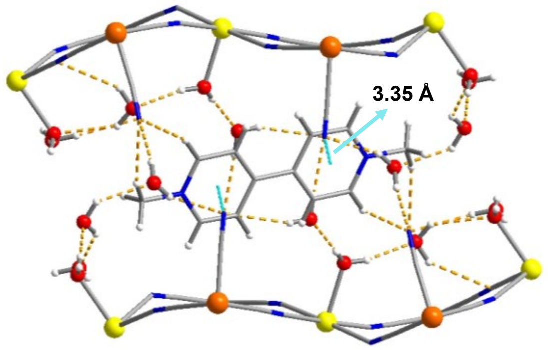

**Figure S4.** The H-bonds interactions (yellow dash line) and anion-$\pi$ interactions (blue dash line) of **FeMn**. Color codes: Fe, orange; Mn, yellow; N, blue; O, red; C, grey; H, white.

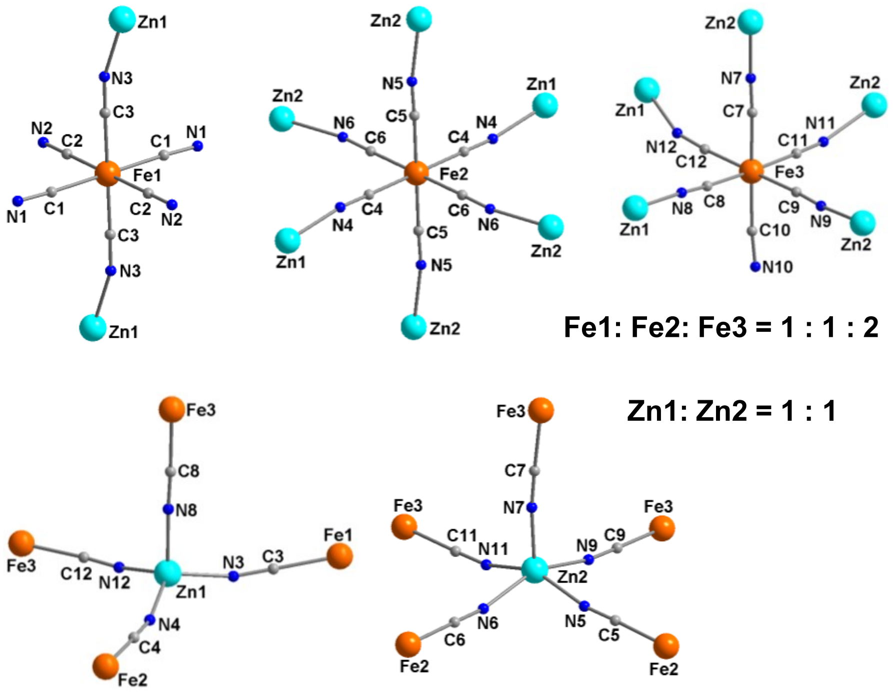

**Figure S5.** The coordination environment of different crystallographic independent Fe ions and Zn ions in **FeZn**.

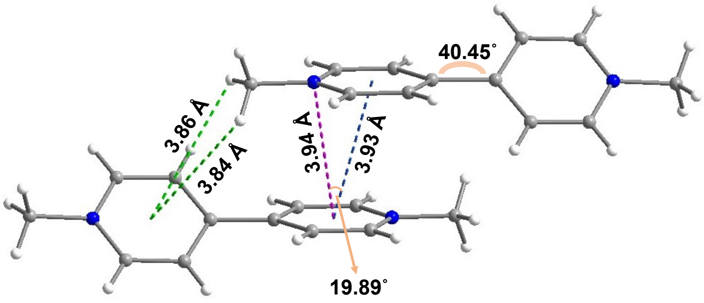

**Figure S6.** The C-H$\cdots\pi$ interactions (green dash line), cation-$\pi$ interactions (purple dash line), $\pi\cdots\pi$ interactions (blue dash line), and dihedral angles between two adjacent pyridine rings of **FeZn**. Color codes: N, blue; C, grey; H, white.

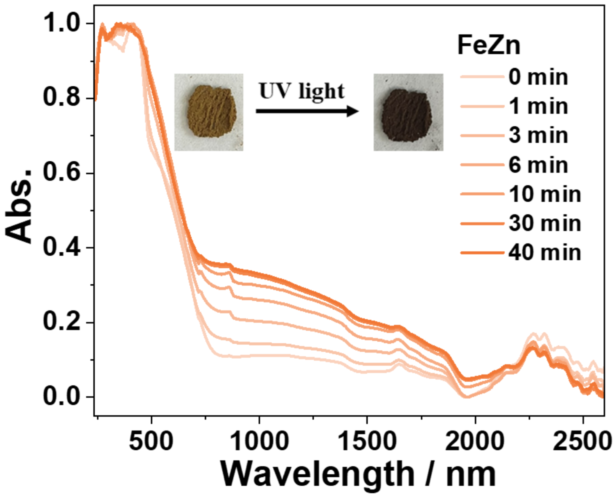

**Figure S7.** Time-dependent UV-Vis-NIR diffuse reflectance spectra and photographs of **FeZn** upon irradiation with 365 nm UV light at room temperature. Different from that under Xe lamp irradiation, the photochromism of **FeZn** under UV light exhibits slower conversion and less absorption between 750 and 2000 nm. The increase of absorption stopped in around 30 min. Therefore, we attribute this observation to the incomplete photochromism of **FeZn-UV** compared to **FeZn-P**.

**Figure S8.** The single crystal photographs of **FeZn** upon irradiation with 365 nm UV light at room temperature.

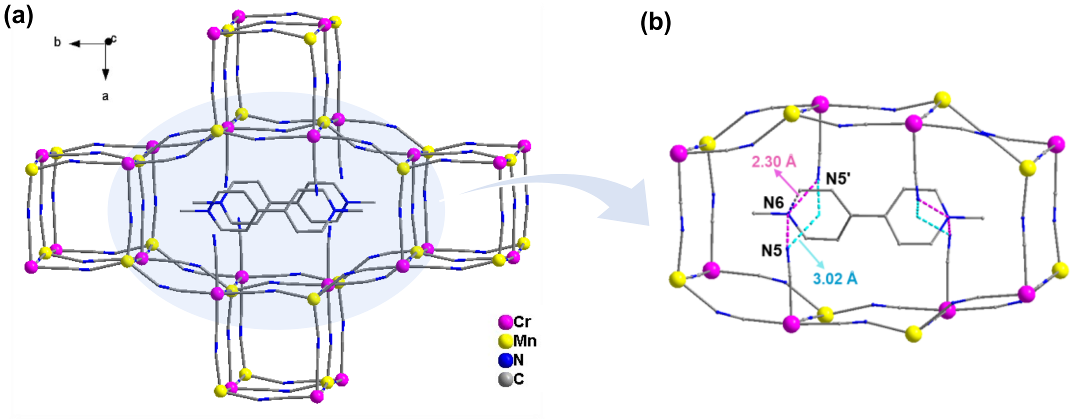

**Figure S9.** (a) Crystal structure of **CrMn**. (b) The direct electron transfer channels (purple dash line) and indirect electron transfer channels (blue dash line) of **CrMn**.

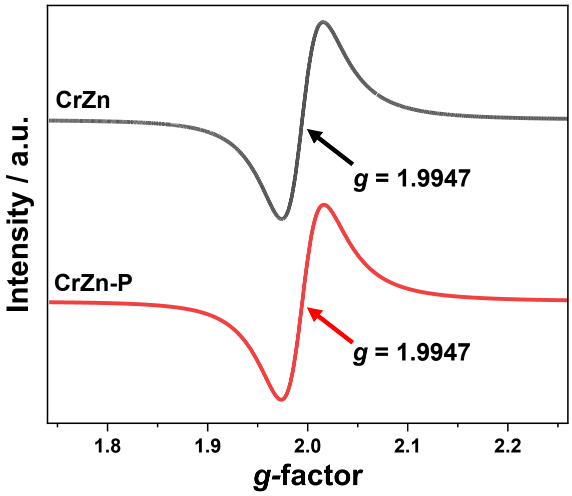

**Figure S10.** The EPR spectra for **CrZn** and **CrZn-P** at room temperature.

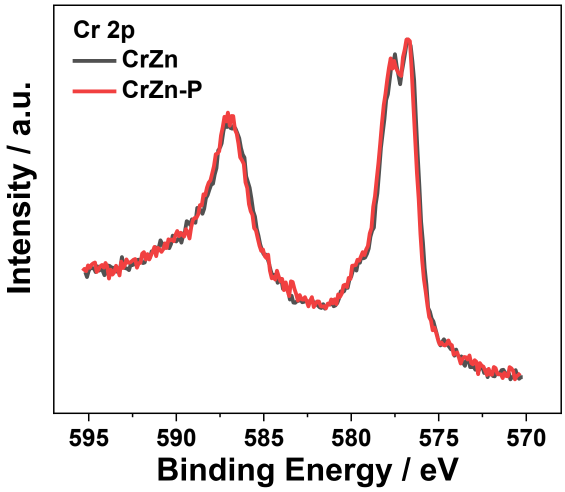

**Figure S11.** The XPS Cr 2p core-level spectra for **CrZn** and **CrZn-P** at room temperature.

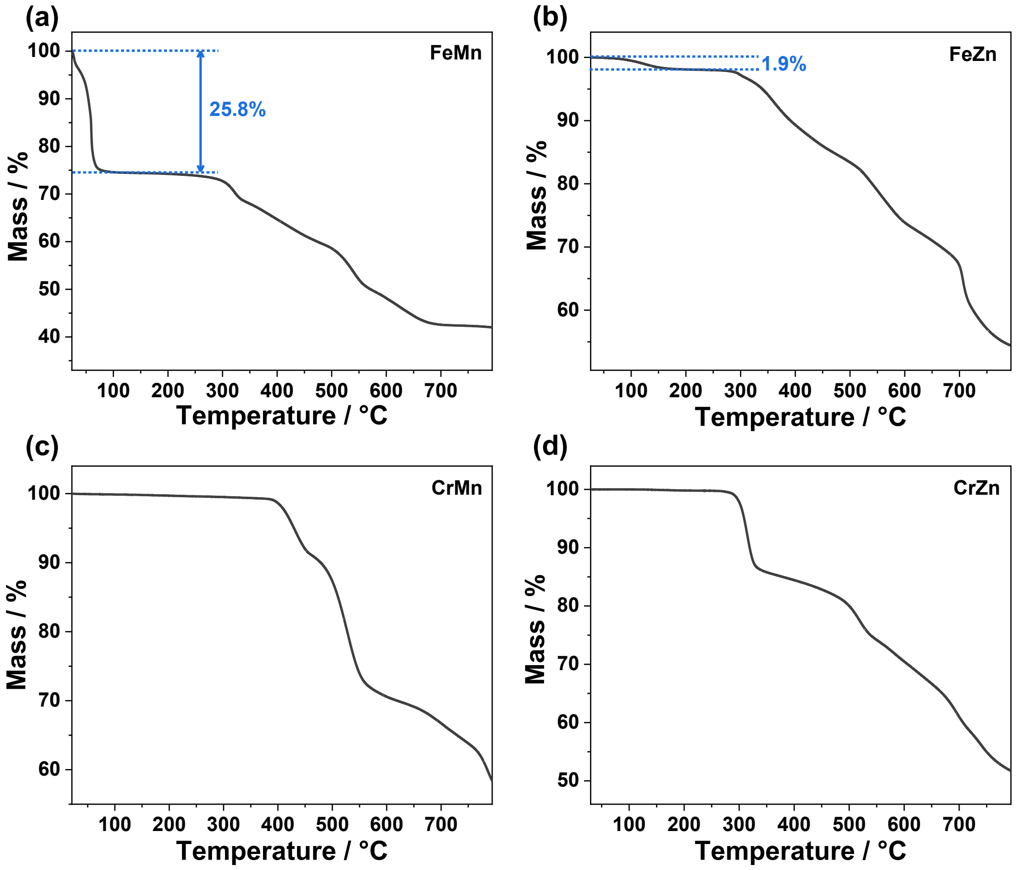

**Figure S12.** Thermogravimetric analysis for **FeMn** (a), **FeZn** (b), **CrMn** (c), and **CrZn** (d).

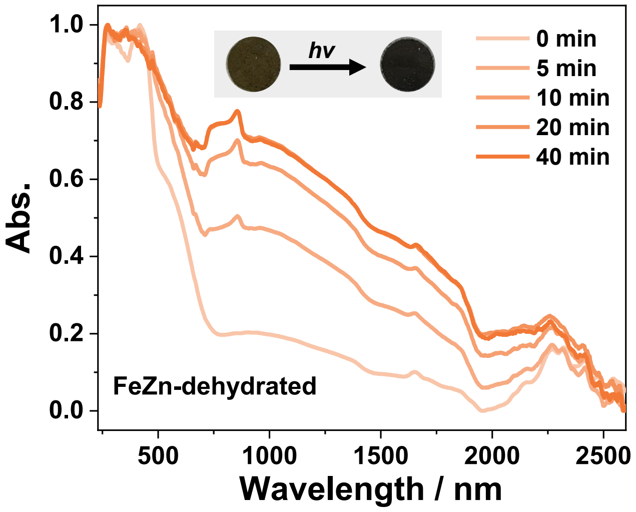

**Figure S13.** Time-dependent UV-Vis-NIR diffuse reflectance spectra of **FeZn-dehydrated** upon irradiation at room temperature.

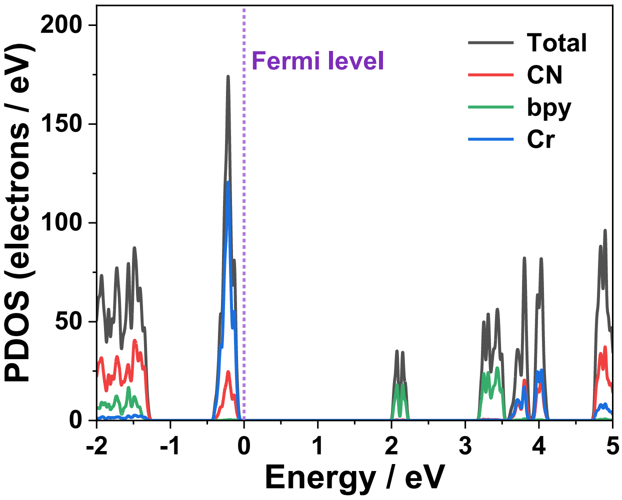

**Figure S14.** Partial density of states (DOSs) for **CrZn**, where CN represents the sum of all states of CN groups from $Cr(CN)_6^{3-}$ groups, bpy represents the sum of all states of bipyridine rings from viologens, Cr represents the sum of all states of $Cr^{3+}$ions from $Cr(CN)_6^{3-}$ groups.

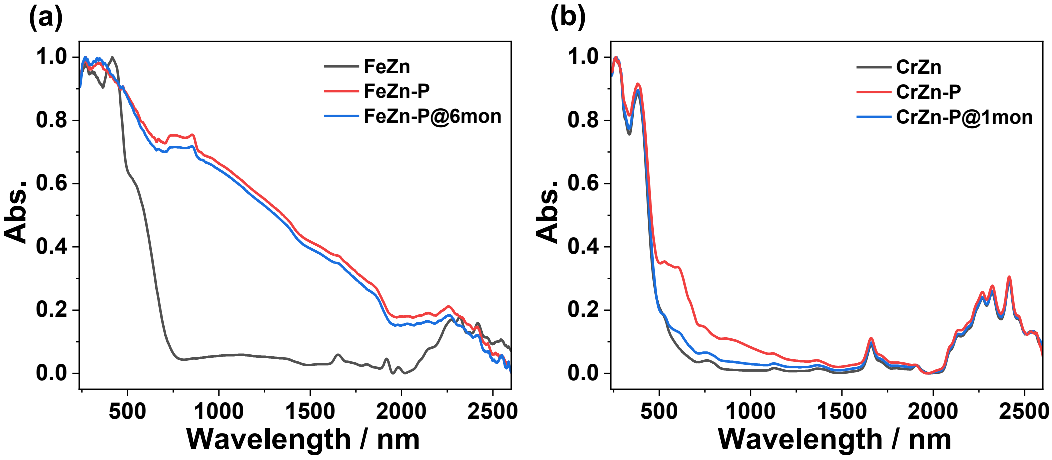

**Figure S15.** Stability test for **FeZn-P** (a) and **CrZn-P** (b) by UV-Vis-NIR diffuse reflectance spectra.

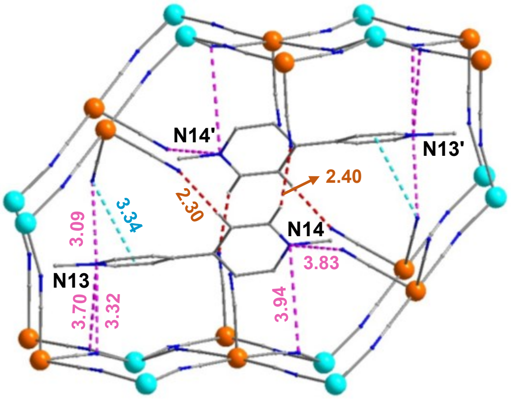

**Figure S16.** The direct electron transfer channels (purple dash line) and indirect electron transfer interactions (blue and yellow dash line) of **FeZn**. Color codes: Fe, orange; Zn, cyan; N, blue; C, grey.

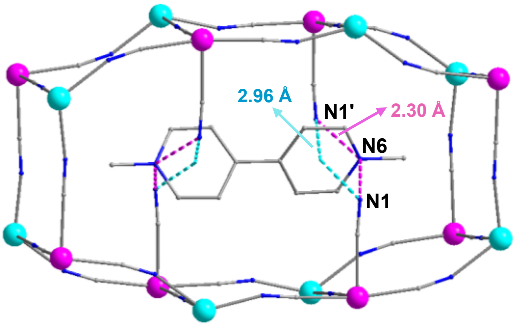

**Figure S17.** The direct electron transfer channels (purple dash line) and indirect electron transfer interactions (blue dash line) of **CrZn**. Color codes: Cr, purple; Zn, cyan; N, blue; C, grey.

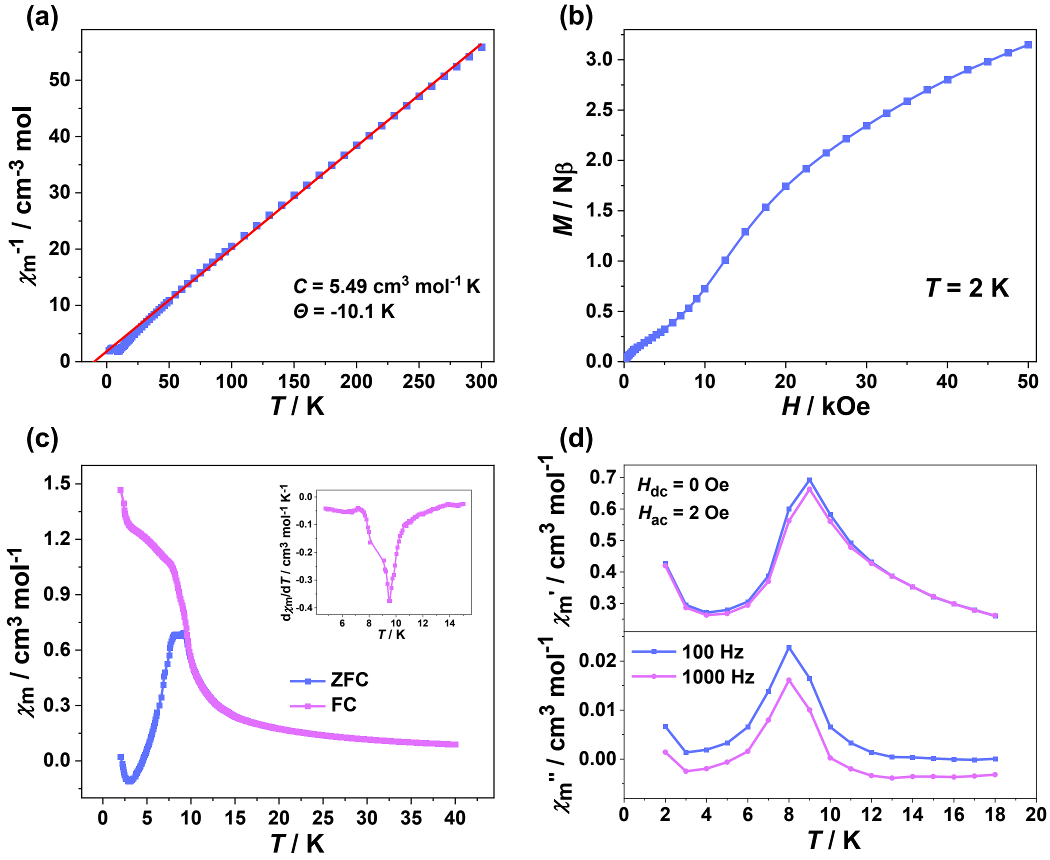

**Figure S18.** Magnetic properties for **FeMn**. (a) Temperature dependence of $\chi_m^{-1}$ at 1 kOe dc field. The red line is the fitting to Curie-Weiss law at 28-300 K. (b) Plot of magnetization *M* vs *H* at 2 K. (c) Plots of ZFC-FC at 100 Oe dc field, inset shows the differentiation of the FC plot. (d) Temperature-dependence of the in-phase ($\chi'_m$) and out-of-phase ($\chi''_m$) susceptibilities under 2 Oe ac field and zero dc field.

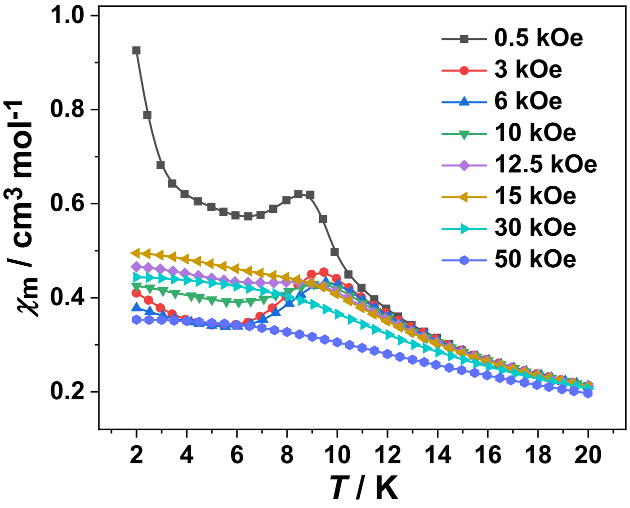

**Figure S19.** Plots of FC for **FeMn** at different dc fields.

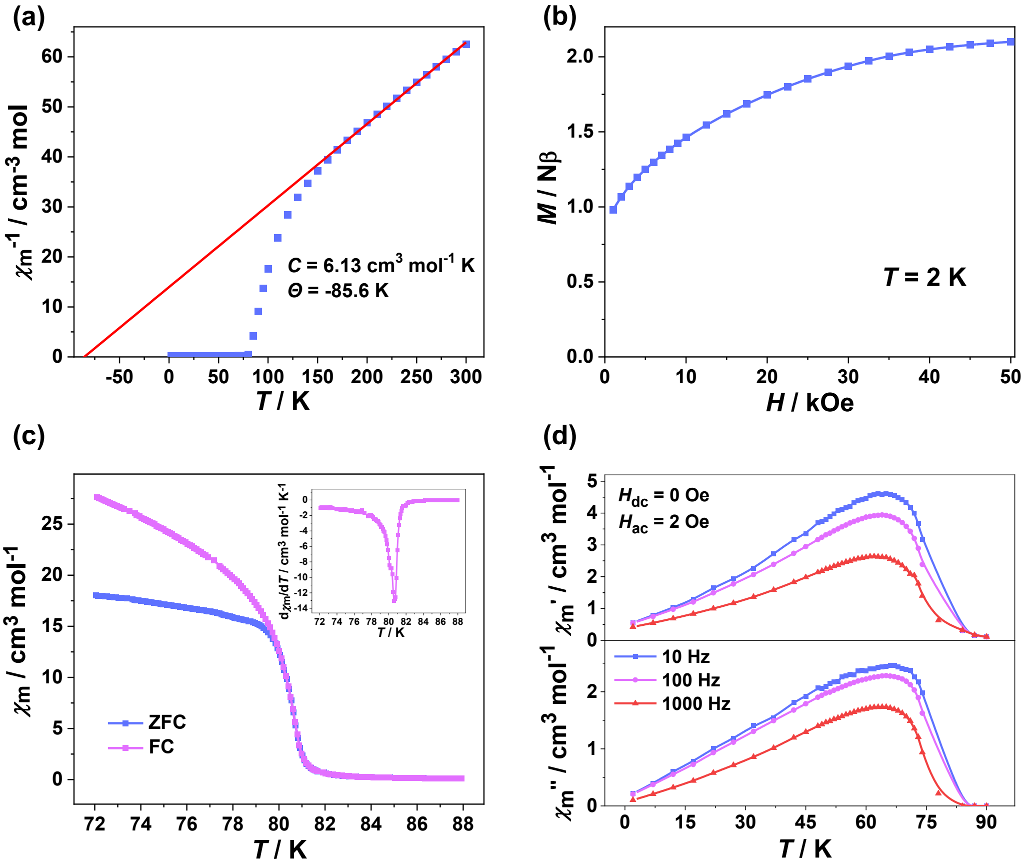

**Figure S20.** Magnetic properties for **CrMn**. (a) Temperature dependence of $\chi_m^{-1}$ at 1 kOe dc field. The red line is the fitting to Curie-Weiss law at 160-300 K. (b) Plot of magnetization *M* vs *H* at 2 K. (c) Plots of ZFC-FC at 100 Oe dc field, inset shows the differentiation of the FC plot. (d) Temperature-dependence of the in-phase ($\chi'_m$) and out-of-phase ($\chi''_m$) susceptibilities under 2 Oe ac field and zero dc field.

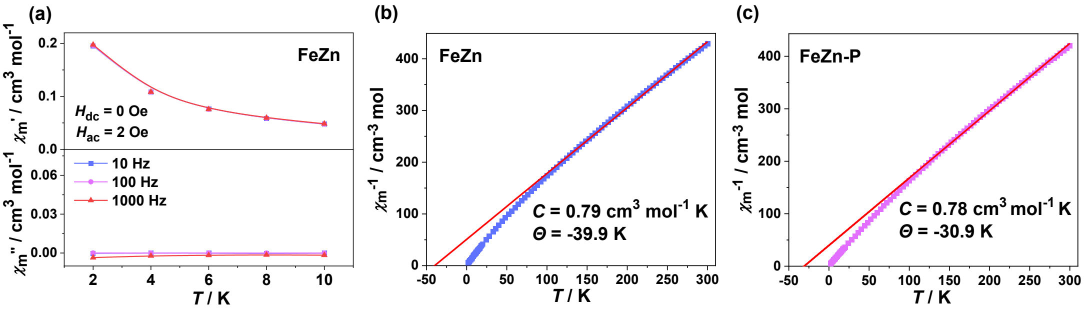

**Figure S21.** Magnetic properties for **FeZn** and **FeZn-P**. (a) Temperature-dependence of the in-phase ($\chi'_m$) and out-of-phase ($\chi''_m$) susceptibilities for **FeZn** under 2 Oe ac field and zero dc field. Temperature dependence of $\chi_m^{-1}$ for **FeZn** (b) and **FeZn-P** (c) at 1 kOe dc field. The red line is the fitting to Curie-Weiss law at 100-300 K.

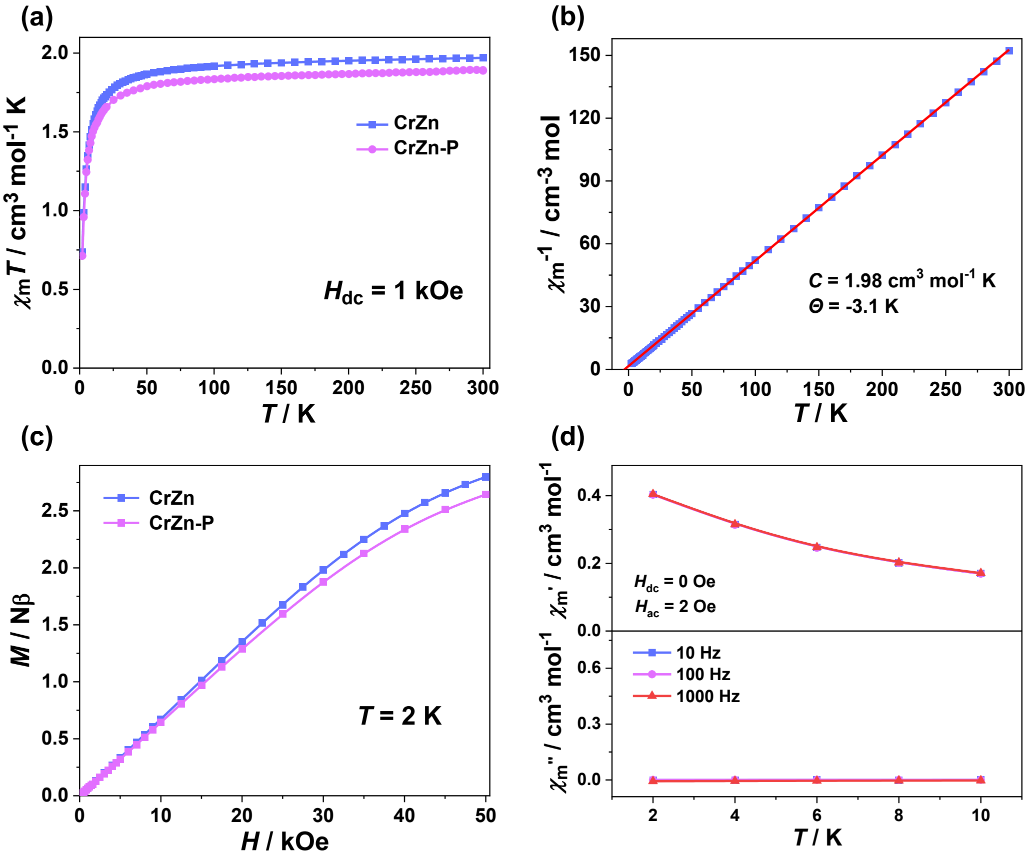

**Figure S22.** Magnetic properties for **CrZn** and **CrZn-P**. (a) Temperature dependence of $\chi_m T$ for **CrZn** and **CrZn-P** at 1 kOe dc field. (b) Temperature dependence of $\chi_m^{-1}$ for **CrZn** at 1 kOe dc field. The red line is the fitting to Curie-Weiss law at 2-300 K. (c) Plots of magnetization $M$ vs $H$ for **CrZn** and **CrZn-P** at 2 K. (d) Temperature-dependence of the in-phase ($\chi'_m$) and out-of-phase ($\chi''_m$) susceptibilities for **CrZn** under 2 Oe ac field and zero dc field.

**Table S1.** Crystallographic Data and Structural Refinements Parameters for **FeMn**, **FeZn**, **CrMn**, **CrZn** and **FeZn-UV**.

| Compound | **FeMn** | **FeZn** | **CrMn** | **CrZn** | **FeZn-UV** |
|---|---|---|---|---|---|
| Formula | $C_{12}H_{21}N_7O_7FeMn$ | $C_{24}H_{16}N_{14}OFe_2Zn_2$ | $C_{12}H_7N_7CrMn$ | $C_{12}H_7N_7CrZn$ | $C_{24}H_{16}N_{14}OFe_2Zn_2$ |
| *Mr* | 486.15 | 758.95 | 356.19 | 366.62 | 758.95 |
| T / K | 180 | 180 | 180 | 180 | 90 |
| Crystal system | monoclinic | triclinic | orthorhombic | orthorhombic | triclinic |
| Space group | $P2_1/c$ | $P\bar{1}$ | *Ibam* | *Ibam* | $P\bar{1}$ |
| $a$ [Å] | 7.3543(2) | 7.3871(1) | 14.2605(6) | 20.0833(10) | 7.3873(2) |
| $b$ [Å] | 14.5105(3) | 12.7783(2) | 20.4255(8) | 14.1046(5) | 12.7497(4) |
| $c$ [Å] | 19.4498(5) | 17.1640(2) | 10.8491(5) | 10.7747(5) | 17.1462(7) |
| $\alpha$ [°] | 90.00 | 96.372(1) | 90.00 | 90.00 | 96.202(3) |
| $\beta$ [°] | 93.973(2) | 99.853(1) | 90.00 | 90.00 | 99.708(3) |
| $\gamma$ [°] | 90.00 | 105.983(1) | 90.00 | 90.00 | 106.140(2) |
| $V$ (Å$^3$) | 2070.59(9) | 1513.05(4) | 3160.1(2) | 3052.1(2) | 1508.46(9) |
| $Z$ | 4 | 2 | 8 | 8 | 2 |
| $\rho$ [g·cm$^{-3}$] | 1.559 | 1.666 | 1.497 | 1.596 | 1.671 |
| $\mu$ [mm$^{-1}$] | 1.357 | 2.550 | 1.488 | 2.286 | 2.558 |
| $F$(000) | 996.0 | 756.0 | 1416.0 | 1456.0 | 756.0 |
| Unique refln. | 3655 | 7358 | 2024 | 1952 | 8555 |
| GOF on $F^2$ | 1.301 | 1.049 | 1.108 | 1.090 | 1.126 |
| $R_1$ [$I$>2σ($I$)] | 0.0276 | 0.0322 | 0.0191 | 0.0227 | 0.0644 |
| $wR_2$ (all data) | 0.0896 | 0.0874 | 0.0534 | 0.0556 | 0.2001 |

**Table S2.** Selected bond lengths (Å) and angles (deg) for **FeMn**.

| **FeMn** | | | |
|---|---|---|---|
| Fe1-C1 | 1.935(3) | C4-Fe1-C2 | 174.80(12) |
| Fe1-C2 | 1.944(3) | C4-Fe1-C3 | 85.99(12) |
| Fe1-C3 | 1.940(3) | C4-Fe1-C5 | 90.56(12) |
| Fe1-C4 | 1.939(3) | C4-Fe1-C6 | 89.30(12) |
| Fe1-C5 | 1.948(3) | C6-Fe1-C2 | 92.13(12) |
| Fe1-C6 | 1.941(3) | C6-Fe1-C5 | 90.94(12) |
| Mn1-N1$^{1}$ | 2.223(3) | N1$^{1}$-Mn1-N3$^{2}$ | 176.75(9) |
| Mn1-N3$^{2}$ | 2.224(2) | N1$^{1}$-Mn1-N5$^{3}$ | 88.93(10) |
| Mn1-N5$^{3}$ | 2.244(3) | N1$^{1}$-Mn1-O2 | 90.30(9) |
| Mn1-N6 | 2.216(3) | N3$^{2}$-Mn1-N5$^{3}$ | 89.24(9) |
| Mn1-O1 | 2.159(2) | N3$^{2}$-Mn1-O2 | 87.08(9) |
| Mn1-O2 | 2.244(2) | N5$^{3}$-Mn1-O2 | 92.23(9) |
| C1-Fe1-C2 | 88.61(12) | N6-Mn1-N1$^{1}$ | 92.86(10) |
| C1-Fe1-C3 | 92.60(12) | N6-Mn1-N3$^{2}$ | 89.04(9) |
| C1-Fe1-C4 | 90.02(12) | N6-Mn1-N5$^{3}$ | 177.74(10) |
| C1-Fe1-C5 | 88.34(11) | N6-Mn1-O2 | 89.15(9) |
| C1-Fe1-C6 | 179.00(12) | O1-Mn1-N1$^{1}$ | 89.11(9) |
| C2-Fe1-C5 | 94.41(12) | O1-Mn1-N3$^{2}$ | 93.62(9) |
| C3-Fe1-C2 | 89.06(12) | O1-Mn1-N5$^{3}$ | 91.43(10) |
| C3-Fe1-C5 | 176.42(12) | O1-Mn1-N6 | 87.22(10) |
| C3-Fe1-C6 | 88.08(12) | O1-Mn1-O2 | 176.29(9) |

Symmetry code: $^{1}$1-X, -1/2+Y, 1/2-Z; $^{2}$-1+X, +Y, +Z; $^{3}$-X, -1/2+Y, 1/2-Z

**Table S3.** The hydrogen bonds for **FeMn** and **FeZn**.

| | **D-H** | **H···A** | **D···A** | **< (DHA)** |
|---|---|---|---|---|
| **FeMn** | | | | |
| O1-H1A···O4 | 0.82 | 1.93 | 2.7324(1) | 167 |
| O1-H1B···O3 | 0.74 | 2.01 | 2.7518(1) | 173 |
| O2-H2A···O5 | 0.82 | 2.13 | 2.9207(1) | 161 |
| O2-H2B···O6 | 0.78 | 1.96 | 2.7190(1) | 167 |
| O3-H3A···N2 | 0.85 | 2.08 | 2.9282(1) | 177 |
| O3-H3B···N2 | 0.76 | 2.51 | 3.2338(1) | 162 |
| O4-H4A···N6 | 0.85 | 2.56 | 3.2943(1) | 145 |
| O4-H4B···O2 | 0.85 | 2.25 | 2.9492(1) | 139 |
| O5-H5B···N4 | 0.85 | 2.25 | 3.0959(1) | 173 |
| O6-H6A···O5 | 0.85 | 2.24 | 2.9041(1) | 135 |
| O6-H6B···O7 | 0.85 | 2.14 | 2.7820(1) | 132 |
| O7-H7A···N4 | 0.85 | 2.03 | 2.8782(1) | 172 |
| O7-H7B···N2 | 0.81 | 2.31 | 3.0838(1) | 159 |
| C11-H11···N4 | 0.93 | 2.57 | 3.4241(1) | 152 |
| C12-H12A···N4 | 0.96 | 2.61 | 3.5103(1) | 156 |
| **FeZn** | | | | |
| O1-H1A···N2 | 0.85 | 2.07 | 2.9076(1) | 168 |
| O1-H1B···N1 | 0.85 | 2.36 | 3.2100(1) | 176 |
| C20-H20···N1 | 0.93 | 2.30 | 3.2149(1) | 169 |
| C21-H21···N10 | 0.93 | 2.40 | 3.2688(1) | 156 |
| C14-H14···O1 | 0.93 | 2.52 | 3.0864(1) | 120 |
| C15-H15···O1 | 0.93 | 2.48 | 3.0687(1) | 121 |
| C22-H22B···O1 | 0.96 | 2.47 | 3.3050(1) | 145 |

**Table S4.** Selected bond lengths (Å) and angles (deg) for **FeZn**.

| **FeZn** | | | | | |
|---|---|---|---|---|---|
| Fe1-C1$^{5}$ | 1.944(3) | C1-Fe1-C2 | 88.36(10) | C8-Fe3-C9 | 87.54(9) |
| Fe1-C1 | 1.944(3) | C1$^{5}$-Fe1-C2 | 91.64(10) | C8-Fe3-C10 | 93.78(9) |
| Fe1-C2 | 1.955(2) | C2$^{5}$-Fe1-C2 | 180.0 | C8-Fe3-C11 | 176.72(9) |
| Fe1-C2$^{5}$ | 1.955(2) | C3-Fe1-C1$^{5}$ | 90.06(10) | C8-Fe3-C12 | 89.96(9) |
| Fe1-C3$^{5}$ | 1.910(2) | C3$^{5}$-Fe1-C1 | 90.06(10) | C9-Fe3-C10 | 87.27(9) |
| Fe1-C3 | 1.910(2) | C3$^{5}$-Fe1-C1$^{5}$ | 89.94(10) | C11-Fe3-C7 | 90.67(8) |
| Fe2-C4$^{6}$ | 1.932(2) | C3-Fe1-C1 | 89.94(10) | C11-Fe3-C9 | 91.86(8) |
| Fe2-C4 | 1.932(2) | C3$^{5}$-Fe1-C2 | 92.06(9) | C11-Fe3-C10 | 89.41(9) |
| Fe2-C5 | 1.943(2) | C3-Fe1-C2 | 87.94(9) | C11-Fe3-C12 | 90.52(8) |
| Fe2-C5$^{6}$ | 1.943(2) | C3-Fe1-C2$^{5}$ | 92.06(9) | C12-Fe3-C7 | 86.96(9) |
| Fe2-C6 | 1.950(2) | C3$^{5}$-Fe1-C2$^{5}$ | 87.94(9) | C12-Fe3-C9 | 176.83(9) |
| Fe2-C6$^{6}$ | 1.950(2) | C3$^{5}$-Fe1-C3 | 180.00(11) | C12-Fe3-C10 | 94.85(9) |
| Fe3-C7 | 1.937(2) | C4-Fe2-C4$^{6}$ | 180.000(1) | N3-Zn1-N4 | 115.60(8) |
| Fe3-C8 | 1.928(2) | C4-Fe2-C5 | 89.99(8) | N3-Zn1-N8$^{1}$ | 99.49(8) |
| Fe3-C9 | 1.938(2) | C4$^{6}$-Fe2-C5 | 90.01(8) | N3-Zn1-N12 | 116.46(8) |
| Fe3-C10 | 1.946(2) | C4$^{6}$-Fe2-C5$^{6}$ | 89.99(8) | N4-Zn1-N8$^{1}$ | 107.14(8) |
| Fe3-C11 | 1.932(2) | C4-Fe2-C5$^{6}$ | 90.01(8) | N12-Zn1-N4 | 112.40(8) |
| Fe3-C12 | 1.936(2) | C4-Fe2-C6 | 88.15(8) | N12-Zn1-N8$^{1}$ | 103.59(8) |
| Zn1-N3 | 1.9434(19) | C4-Fe2-C6$^{6}$ | 91.85(8) | N5$^{2}$-Zn2-N6 | 86.09(7) |
| Zn1-N4 | 1.9819(18) | C4$^{6}$-Fe2-C6$^{6}$ | 88.15(8) | N7-Zn2-N5$^{2}$ | 103.45(8) |
| Zn1-N8$^{1}$ | 1.9955(19) | C4$^{6}$-Fe2-C6 | 91.85(8) | N7-Zn2-N6 | 102.36(8) |
| Zn1-N12 | 1.9573(18) | C5-Fe2-C5$^{6}$ | 180.00(12) | N7-Zn2-N9$^{3}$ | 101.32(8) |
| Zn2-N5$^{2}$ | 2.1016(18) | C5-Fe2-C6 | 91.68(8) | N7-Zn2-N11$^{4}$ | 103.34(8) |
| Zn2-N6 | 2.1379(18) | C5$^{6}$-Fe2-C6$^{6}$ | 91.68(8) | N9$^{3}$-Zn2-N5$^{2}$ | 86.09(7) |
| Zn2-N7 | 1.9903(18) | C5$^{6}$-Fe2-C6 | 88.32(8) | N9$^{3}$-Zn2-N6 | 156.20(7) |
| Zn2-N9$^{3}$ | 2.0896(18) | C5-Fe2-C6$^{6}$ | 88.32(8) | N11$^{4}$-Zn2-N5$^{2}$ | 153.18(7) |
| Zn2-N11$^{4}$ | 2.0598(18) | C6-Fe2-C6$^{6}$ | 180.00(11) | N11$^{4}$-Zn2-N6 | 87.01(7) |
| C1-Fe1-C1$^{5}$ | 180.00(14) | C7-Fe3-C9 | 90.92(9) | N11$^{4}$-Zn2-N9$^{3}$ | 89.92(7) |
| C1-Fe1-C2$^{5}$ | 91.64(10) | C7-Fe3-C10 | 178.19(19) | | |
| C1$^{5}$-Fe1-C2$^{5}$ | 88.36(10) | C8-Fe3-C7 | 86.11(9) | | |

Symmetry code: $^{1}$-1+X, +Y, +Z; $^{2}$1+X, +Y, +Z; $^{3}$3-X, 2-Y, 1-Z; $^{4}$2-X, 2-Y, 1-Z; $^{5}$-X, 1-Y, -Z; $^{6}$1-X, 1-Y, 1-Z

**Table S5.** Selected bond lengths (Å) and angles (deg) for **FeZn-UV**.

| **FeZn-UV** | | | | | |
|---|---|---|---|---|---|
| Fe1-C1$^{6}$ | 1.957(11) | C3-Fe1-C1 | 91.6(4) | C7-Fe3-C12 | 87.1(4) |
| Fe1-C1 | 1.957(11) | C3$^{6}$-Fe1-C1 | 88.4(4) | C7-Fe3-C9 | 90.6(4) |
| Fe1-C2 | 1.950(11) | C3$^{6}$-Fe1-C3 | 180.0 | C7-Fe3-C10 | 177.9(4) |
| Fe1-C2$^{6}$ | 1.950(11) | C3$^{6}$-Fe1-C2 | 90.3(5) | C8-Fe3-C12 | 90.2(4) |
| Fe1-C3 | 1.923(10) | C3-Fe1-C2$^{6}$ | 90.3(5) | C8-Fe3-C9 | 92.1(4) |
| Fe1-C3$^{6}$ | 1.923(10) | C3-Fe1-C2 | 89.7(5) | C8-Fe3-C10 | 89.2(4) |
| Fe2-C4 | 1.932(8) | C3$^{6}$-Fe1-C2$^{6}$ | 89.7(5) | C8-Fe3-C7 | 90.1(4) |
| Fe2-C4$^{3}$ | 1.932(8) | C2-Fe1-C1 | 88.2(4) | C8-Fe3-C11 | 176.7(4) |
| Fe2-C5$^{3}$ | 1.942(9) | C2-Fe1-C1$^{6}$ | 91.8(4) | C11-Fe3-C12 | 90.0(3) |
| Fe2-C5 | 1.942(9) | C2$^{6}$-Fe1-C1 | 91.8(4) | C11-Fe3-C9 | 87.6(4) |
| Fe2-C6$^{3}$ | 1.951(10) | C2$^{6}$-Fe1-C1$^{6}$ | 88.3(4) | C11-Fe3-C10 | 94.1(4) |
| Fe2-C6 | 1.951(10) | C2-Fe1-C2$^{6}$ | 180.0 | C11-Fe3-C7 | 86.6(4) |
| Fe3-C7 | 1.940(9) | C4$^{3}$-Fe2-C4 | 180.0 | N12-Zn1-N4 | 112.7(3) |
| Fe3-C8 | 1.927(9) | C4$^{3}$-Fe2-C5$^{3}$ | 90.3(4) | N12-Zn1-N11$^{5}$ | 103.5(3) |
| Fe3-C9 | 1.941(9) | C4-Fe2-C5$^{3}$ | 89.7(4) | N4-Zn1-N11$^{5}$ | 107.0(3) |
| Fe3-C10 | 1.949(9) | C4$^{3}$-Fe2-C5 | 89.7(4) | N3-Zn1-N12 | 116.2(3) |
| Fe3-C11 | 1.930(9) | C4-Fe2-C5 | 90.3(4) | N3-Zn1-N4 | 115.5(3) |
| Fe3-C12 | 1.941(9) | C4$^{3}$-Fe2-C6$^{3}$ | 91.6(4) | N3-Zn1-N11$^{5}$ | 99.7(3) |
| Zn1-N12 | 1.960(8) | C4-Fe2-C6 | 91.6(4) | N7-Zn2-N9$^{1}$ | 101.6(3) |
| Zn1-N4 | 1.985(8) | C4$^{3}$-Fe2-C6 | 88.4(4) | N7-Zn2-N5$^{2}$ | 103.5(3) |
| Zn1-N3 | 1.945(9) | C4-Fe2-C6$^{3}$ | 88.4(4) | N7-Zn2-N6$^{3}$ | 101.7(3) |
| Zn1-N11$^{5}$ | 1.994(8) | C5$^{3}$-Fe2-C5 | 180.0 | N7-Zn2-N8$^{4}$ | 103.4(3) |
| Zn2-N7 | 1.987(7) | C5$^{3}$-Fe2-C6$^{3}$ | 88.7(3) | N9$^{1}$-Zn2-N5$^{2}$ | 86.1(3) |
| Zn2-N9$^{1}$ | 2.092(8) | C5-Fe2-C6 | 88.7(3) | N9$^{1}$-Zn2-N6$^{3}$ | 156.6(3) |
| Zn2-N5$^{2}$ | 2.095(8) | C5-Fe2-C6$^{3}$ | 91.3(3) | N5$^{2}$-Zn2-N6$^{3}$ | 86.9(3) |
| Zn2-N6$^{3}$ | 2.123(8) | C5$^{3}$-Fe2-C6 | 91.3(3) | N8$^{4}$-Zn2-N9$^{1}$ | 89.4(3) |
| Zn2-N8$^{4}$ | 2.065(8) | C6$^{3}$-Fe2-C6 | 180.0 | N8$^{4}$-Zn2-N5$^{2}$ | 153.1(3) |
| C1$^{6}$-Fe1-C1 | 180.0 | C12-Fe3-C9 | 176.8(4) | N8$^{4}$-Zn2-N6$^{3}$ | 86.8(3) |
| C3-Fe1-C1$^{6}$ | 88.4(4) | C12-Fe3-C10 | 94.9(4) | | |
| C3$^{6}$-Fe1-C1$^{6}$ | 91.6(4) | C9-Fe3-C10 | 87.4(4) | | |

Symmetry code: $^{1}$-1-X, -Y, -Z; $^{2}$-1+X, +Y, +Z; $^{3}$1-X, 1-Y, -Z; $^{4}$-X, -Y, -Z; $^{5}$1+X, +Y, +Z; $^{6}$2-X, 1-Y, 1-Z

**Table S6.** Selected bond lengths (Å) and angles (deg) for **CrMn**.

| **CrMn** | | | |
|---|---|---|---|
| Cr1-C1 | 2.0819(17) | C3-Cr1-C2$^{1}$ | 89.66(3) |
| Cr1-C2 | 2.0811(12) | C3-Cr1-C2 | 89.66(3) |
| Cr1-C2$^{1}$ | 2.0811(12) | C3-Cr1-C4 | 173.04(7) |
| Cr1-C3 | 2.0739(16) | C5-Cr1-C1 | 177.19(6) |
| Cr1-C4 | 2.0837(15) | C5-Cr1-C2$^{1}$ | 91.92(3) |
| Cr1-C5 | 2.0568(17) | C5-Cr1-C2 | 91.92(3) |
| Mn1-N1 | 2.1236(14) | C5-Cr1-C3 | 88.98(7) |
| Mn1-N2$^{2}$ | 2.2044(11) | C5-Cr1-C4 | 84.07(6) |
| Mn1-N2$^{3}$ | 2.2044(11) | N1-Mn1-N2$^{2}$ | 94.11(3) |
| Mn1-N3$^{4}$ | 2.1334(14) | N1-Mn1-N2$^{3}$ | 94.11(3) |
| Mn1-N4$^{5}$ | 2.1877(14) | N1-Mn1-N3$^{4}$ | 109.26(6) |
| C1-Cr1-C4 | 93.13(6) | N1-Mn1-N4$^{5}$ | 121.71(6) |
| C2-Cr1-C1 | 88.10(3) | N2$^{3}$-Mn1-N2$^{2}$ | 170.29(5) |
| C2$^{1}$-Cr1-C1 | 88.10(3) | N3$^{4}$-Mn1-N2$^{3}$ | 91.08(3) |
| C2-Cr1-C2$^{1}$ | 176.08(6) | N3$^{4}$-Mn1-N2$^{2}$ | 91.08(3) |
| C2-Cr1-C4 | 90.58(3) | N3$^{4}$-Mn1-N4$^{5}$ | 129.03(6) |
| C2$^{1}$-Cr1-C4 | 90.58(3) | N4$^{5}$-Mn1-N2$^{3}$ | 85.64(3) |
| C3-Cr1-C1 | 93.83(6) | N4$^{5}$-Mn1-N2$^{2}$ | 85.64(3) |

Symmetry code: $^{1}$+X, +Y, 1-Z; $^{2}$1-X, +Y, -1/2+Z; $^{3}$1-X, +Y, 3/2-Z; $^{4}$1-X, 1-Y, 1-Z; $^{5}$1/2+X, 1/2-Y, +Z

**Table S7.** Selected bond lengths (Å) and angles (deg) for **CrZn**.

| **CrZn** | | | |
|---|---|---|---|
| Cr1-C1 | 2.057(2) | C2-Cr1-C4$^{4}$ | 87.96(4) |
| Cr1-C2$^{3}$ | 2.0841(16) | C2-Cr1-C5$^{5}$ | 90.80(4) |
| Cr1-C2 | 2.0841(16) | C2$^{3}$-Cr1-C5$^{5}$ | 90.80(4) |
| Cr1-C3 | 2.077(2) | C3-Cr1-C2 | 89.51(4) |
| Cr1-C4$^{4}$ | 2.089(2) | C3-Cr1-C2$^{3}$ | 89.51(4) |
| Cr1-C5$^{5}$ | 2.093(2) | C3-Cr1-C4$^{4}$ | 93.63(8) |
| Zn1-N2$^{1}$ | 2.1657(15) | C3-Cr1-C5$^{5}$ | 171.42(9) |
| Zn1-N2$^{2}$ | 2.1657(15) | C4$^{4}$-Cr1-C5$^{5}$ | 94.95(8) |
| Zn1-N3 | 2.026(2) | N2$^{1}$-Zn1-N2$^{2}$ | 171.15(7) |
| Zn1-N4 | 2.0185(19) | N3-Zn1-N2$^{2}$ | 90.52(4) |
| Zn1-N5 | 2.0706(18) | N3-Zn1-N2$^{1}$ | 90.52(4) |
| C1-Cr1-C2$^{3}$ | 92.06(4) | N3-Zn1-N5 | 131.23(8) |
| C1-Cr1-C2 | 92.06(4) | N4-Zn1-N2$^{1}$ | 93.98(3) |
| C1-Cr1-C3 | 88.37(9) | N4-Zn1-N2$^{2}$ | 93.98(3) |
| C1-Cr1-C4$^{4}$ | 177.99(9) | N4-Zn1-N3 | 108.98(8) |
| C1-Cr1-C5$^{5}$ | 83.05(9) | N4-Zn1-N5 | 119.79(8) |
| C2-Cr1-C2$^{3}$ | 175.73(8) | N5-Zn1-N2$^{1}$ | 86.35(3) |
| C2$^{3}$-Cr1-C4$^{4}$ | 87.96(4) | N5-Zn1-N2$^{2}$ | 86.35(3) |

Symmetry code: $^{1}$1-X, +Y, 1/2-Z; $^{2}$1-X, +Y, 1/2+Z; $^{3}$+X, +Y, 1-Z; $^{4}$1-X, 1-Y, 1-Z; $^{5}$-1/2+X, 1/2-Y, +Z

## Mössbauer Spectroscopy Analysis

Due to limited conditions, two constraints or approximations were employed to prevent overparameterization. Firstly, the contribution from internal field of Fe$^{III}$ was omitted as the major spectral features are quadrupole doublets, indicating the fast-relaxation limit is a valid approach. Secondly, guided by the crystal structure, the model for **FeZn** consists of three Fe sites with a ratio constrained to 1:1:2.

Our simulation commenced with a direct comparison between the spectrum for **FeZn** and **FeZn-P**. The difference spectrum (Figure 3b, bottom) clearly suggests that the newly formatted species shows a very narrow doublet. Additionally, the major missing features can also be accounted for by quadrupole doublets. These observations provided the initial parameters of at least two distinct species.

Based on the initial guess, the two spectra were simulated together. To avoid overparameterization, the newly generated narrow doublet was assigned as one species. Consequently, the model for **FeZn-P** consists of four Fe sites: the three sites from **FeZn**, albeit with possibly reduced relative ratio, and one new site corresponding to the newly generated species. The total decreases in the three sites are constrained equal to the amount in the new site. The obtained parameters are listed in Table S8.

**Table S8.** Simulation parameters of $^{57}$Fe Mössbauer spectra for **FeZn** and **FeZn-P**.

| **FeZn** | $\delta$ (mm/s) | $\lvert\Delta E_Q\rvert$ (mm/s) | Relative Area (%) |
|---|---|---|---|
| Site I | -0.16 | 0.80 | 24 |
| Site II | -0.18 | 2.25 | 24 |
| Site III | -0.18 | 1.21 | 49 |
| **FeZn-P** | $\delta$ (mm/s) | $\lvert\Delta E_Q\rvert$ (mm/s) | Relative Area (%) |
| Site I | -0.16 | 0.80 | 24 |
| Site II | -0.18 | 2.25 | 26 |
| Site III | -0.18 | 1.21 | 25 |
| Site IV | -0.12 | 0.20 | 24 |

Isomer shift ($\delta$) generally serves as a good probe of Fe redox activity when their coordination environments are similar. Removing electrons from 3d orbitals generally decreases $\delta$ (more negative). However, for $[Fe(CN)_6]^{x+}$ species, isomer shift changes very little upon Fe reduction or oxidation, as the changes in backdonation upon redox activity can compensate for changes in the number of 3d electrons. For example, the isomer shift of $K_3[Fe(CN)_6]$ and $K_4[Fe(CN)_6]$ are almost identical.[3] As expected, the isomer shift values of the four Fe sites are very close, falling into the range of $[Fe(CN)_6]^{x+}$ (x = 2 or 3) species. Although the isomer shift of Site IV is slightly more positive than the other three, it does not exclusively indicate Fe valence reduction.

In addition, the quadruple splitting ($|\Delta E_Q|$) of $K_3[Fe(CN)_6]$ and $K_4[Fe(CN)_6]$ are also very similar. Quadrupole splitting describes the anisotropy of the electric field gradient (EFG) at the $^{57}$Fe nuclei. The EFG tensor primarily arises from the local contribution of the valence electrons. For low spin (LS) $Fe^{II}$ in an $O_h$ ligand field, the fully occupied $t_{2g}$ molecular orbitals provide an isotropic EFG, yielding a small quadrupole splitting. For example, the quadrupole splitting is undetectable for $K_4[Fe(CN)_6]$. LS $Fe^{III}$ species usually exhibit a large quadrupole splitting as the single unpair electron provides a large anisotropic valence contribution to the EFG tensor. However, for $[Fe(CN)_6]^{3-}$, due to the near $O_h$ symmetry, the $(t_{2g})^5$ configuration yields very low-lying excited states as the $t_{2g}$ orbitals are heavily mixed $d_{xy}$, $d_{yz}$, and $d_{xz}$ orbitals. The valence contribution yields a less anisotropic EFG tensor than the other LS $Fe^{III}$ species.[4]

Unlike $K_3[Fe(CN)_6]$, the three crystallographic independent $Fe^{III}$ in **FeZn** are in distinct environments due to the distribution of $Zn^{II}$ (Figure S5), as described in the main text. Due to the short $CN^-$ bridges, connected $Zn^{II}$ strongly influence the MOs of the $Fe(CN)_xZn_y$ moieties (Scheme 1), resulting in different quadrupole splitting for the $^{57}$Fe nuclei. Generally, $Zn^{II}$ can reduce the interaction between $Fe^{III}$ and $CN^-$. For Fe2, perturbations from $Zn^{II}$ ions are more isotropic as the six $Zn^{II}$ ions surrounding are close to cubic symmetry. The symmetry of ligand field almost remained unchanged, leading to a small $|\Delta E_Q|$. For Fe1, the two axial $Zn^{II}$ reduce the ligand field strength along the z direction, raising the energy of $3d_{xz}$ and $3d_{yz}$ based MOs, yielding anisotropic valence contribution to the EFG tensor. For Fe3, the "$Zn^{II}$ hole" in the axial direction raises the energy of $3d_{xy}$ based MO, also yielding anisotropic valence contribution EFG tensor. Compared to Fe1, the strength of the perturbation should be weaker. Thus, the quadrupole splitting of Fe3 should be between those of Fe1 and Fe2.

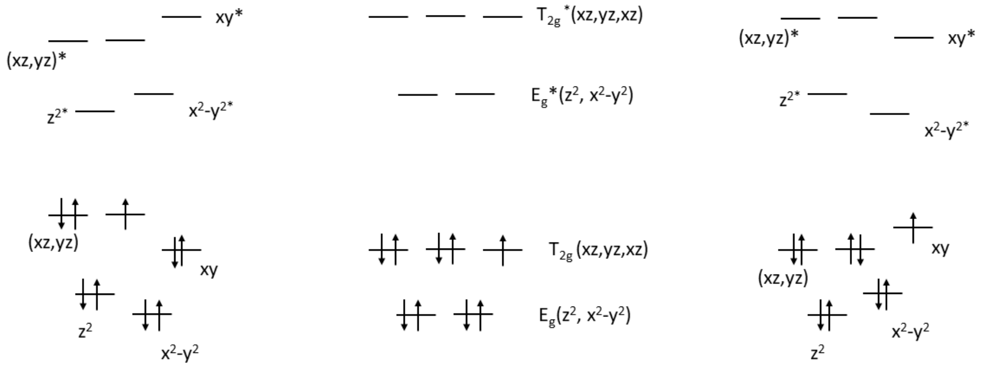

**Scheme 1**. Ligand field variation of $[Fe(CN)_6]^{3-}$ upon addition of two identical cations in the axial direction (left), six identical cations in the axial and equatorial direction (middle), and five identical cations to leave a cation hole in the axial direction (right).

Indeed, our simulations are consistent with the ligand field analysis above. Site I shows a small $|\Delta E_Q|$, while Site II exhibits a large $|\Delta E_Q|$. Site III shows moderate $|\Delta E_Q|$ and accounts for about 50% of the total $^{57}$Fe. Therefore, Site I, II, and III correspond to Fe2, Fe1, and Fe3, respectively. Notably, the $\delta$ of Site I is less negative than the other two sites, consistent with longer average Fe-CN bonds. Longer Fe-CN bonds weaken the back bonding interaction, yielding a less negative isomer shift.

After irradiation, the major change in Fe species is the conversion from Site III to Site IV. The parameters of Site IV highly support that the newly formed Fe species is $Fe^{II}$. The $\delta$ is less negative, and the $|\Delta E_Q|$ is only 0.20 mm/s. As the coordination environment is asymmetric, such close-to-zero $|\Delta E_Q|$ may most possibly come from fulfilled $t_{2g}$ molecular orbitals, which is an intrinsic feature of LS $Fe^{II}$. Combining these two points, our results highly support the assignment of hexacyanido $Fe^{II}$ species.

## References

(1) T. Janoschka, N. Martin, M. D. Hager and U. S. Schubert, An aqueous redox-flow battery with high capacity and power: The TEMPTMA/MV system, *Angew. Chem. Int. Ed.*, 2016, **55**, 14427–14430.

(2) G. Kresse and J. Furthmüller, Efficiency of ab-initio total energy calculations for metals and semiconductors using a plane-wave basis set. *Comput. Mater. Sci*. 1996, **6**, 15–50.

(3) J. H. Enemark and R. D. Feltham, Principles of structure, bonding, and reactivity for metal nitrosyl complexes, *Coord. Chem. Rev.*, 1974, **13**, 339–406.

(4) W. T. Oosterhuis and G. Lang, Mössbauer effect in $K_3Fe(CN)_6$, *Phys. Rev.*, 1969, **178**, 439.